Ionic layered BaFCl and $Ba_{1-x}Sr_xFCl$ compounds: Physical- and chemical-pressure effects

Vincenza D'Anna, Latévi Max Lawson Daku,* and Hans Hagemann
Department of Physical Chemistry, University of Geneva, Quai Ernest Ansermet 30, CH-1211, Geneva 4, Switzerland

Frank Kubel
Institut für Chemische Technologien und Analytik, TU Wien, Getreidemarkt 9/164, A 1060 Vienna, Austria
(Received 6 May 2010; revised manuscript received 5 July 2010; published 27 July 2010)

The effect on crystal structure and vibrational frequencies of physical pressure in BaFCl and chemical pressure in $Ba_{1-x}Sr_xFCl$ solid solutions is studied using periodic density-functional theory (DFT) calculations performed within the local-density approximation (LDA) and the generalized gradient approximation (GGA). These results are compared with previously published experimental data for BaFCl in conjunction with new experimental data for $Ba_{1-x}Sr_xFCl$ and show overall a good agreement with experiment. The GGA method outperforms the LDA method for the description of BaFCl under pressure. However, the two DFT methods perform equally well for the description of the solid solutions, which have been studied within the virtual-crystal approximation. They also give consistent values of the energy of formation of $Ba_{1-x}Sr_xFCl$, which can be correlated with the experimentally observed melting points. The comparison of the calculated mode Grüneisen parameters shows that, for the investigated systems, the effect of the chemical pressure and that of the physical pressure are not identical.

DOI: 10.1103/PhysRevB.82.024108 PACS number(s): 61.50.Ks, 71.15.Mb, 63.20.−e, 61.66.Dk

I. INTRODUCTION

Alkaline-earth fluorohalides (*MFX*) are receiving much attention in material and optical sciences owing to the remarkable photophysical and photochemical properties which they can exhibit upon incorporation of photoactive rare-earth ions. For instance, Eu^{2+}-doped BaF*X* (*X*=Cl,Br,I) compounds are known efficient x-ray storage phosphors,[1–3] and recently, nanocrystalline Sm^{3+}-doped BaFCl was also proposed as an efficient x-ray storage phosphor.[4] Besides this involvement in the field of x-ray imaging, the report of room-temperature persistent hole burning in Sm^{2+}-doped $SrFCl_{0.5}Br_{0.5}$ and $Sr_{0.5}Ba_{0.5}FCl_{0.5}Br_{0.5}$ crystals helped establish such rare-earth-doped mixed compounds as promising candidate materials for the design of high-density optical data storage devices.[5,6] Let us also add that Sm^{2+}-doped BaFCl was shown to be a better pressure sensor than ruby for pressures of up to 10 GPa.[7,8]

The properties of the incorporated rare-earth ions obviously depend on the structure of the *MFX* host. Neat *MFX* compounds crystallize in the tetragonal $P4/nmm$ (no. 129) *Matlockite* structure. That is, they exhibit a layered ionic structure which corresponds to a simple $-F^--M^{2+}-X^--X^--M^{2+}-F^--$ stacking of the ion layers along the *c* axis (Fig. 1). In this structure, the M^{2+} and X^- ions are located at Wyckoff 2*c* positions and the F^- ions at Wyckoff 2*a* positions. This translates into a ninefold coordination of the M^{2+} cations which is depicted in Fig. 2: each cation is coordinated by the equivalent four nearest fluorides from the F^- plane below its plane, by the equivalent four nearest X^- ions from the X^- plane above, and by the next-nearest X^- ion which belongs to the second X^- plane above. The resulting $[MF_4X_5]$ structural motif has a C_{4v} site symmetry and it determines the crystal field experienced by the M^{2+}-substituting rare-earth ions, hence the photophysical properties of these last ones.

There is an extended miscibility between many pairs *MFX* and *M′FX′* ($M \neq M'$ and/or $X \neq X'$) of this crystal family. For instance, and of particular interest to us, the $Sr_xBa_{1-x}FCl_yBr_{1-y}$ $[(x,y) \in [0,1]^2]$ system forms complete solid solutions and the tetragonal Matlockite structure is preserved in the mixed crystals.[9] The possibility to thus readily vary the chemical composition and concomitantly the crystal structure provides an efficient means to fine tune the crystal field at the cation site. This sensitivity of the crystal field to geometric changes is also reflected by the pressure dependence of the luminescence properties of Sm^{2+} in the $BaFCl:Sm^{2+}$ pressure sensor,[8] for example.

It follows that the influence of chemical substitution on the structure of the *MFX* compounds can be thought in terms of an internal or chemical pressure. The concept of chemical pressure is of widespread use in solid-state chemistry and in solid-state physics as it offers an appealing parallel between the effect of the external pressure on a specific property of a material and the effect on this same property of a lattice volume variation obtained by chemical changes. For instance, it helped get insight into the manner in which the relative energies of the ligand-field states of transition metal complexes can be fine tuned by guest-host interactions in confining crystalline environments.[10,11] The concept of chemical pressure was also employed by Sugi *et al.*[12] in their study of the Fermi-surface properties of $CeRu_2(Si_{1-x}Ge_x)_2$ in magnetic fields: the composition parameter *x* of the alloy was used as a measure of the chemical pressure because the magnetic phase diagram of $CeRu_2Ge_2$ under applied pressures of up to 11 GPa is nearly similar to the one of $CeRu_2(Si_{1-x}Ge_x)_2$ as a function of the unit-cell volume. Recently, the similarities between the structural distortions under pressure and chemical doping in superconducting $BaFe_2As_2$ were also evidenced and rationalized in terms of chemical pressure.[13]

In view of the numerous potential uses of the rare-earth-doped *MFX* crystals, it is clearly of both fundamental and technological importance to achieve an in-depth understanding of the influence of pressure and chemical substitution on the structure of the *MFX* hosts. The vibrational properties of

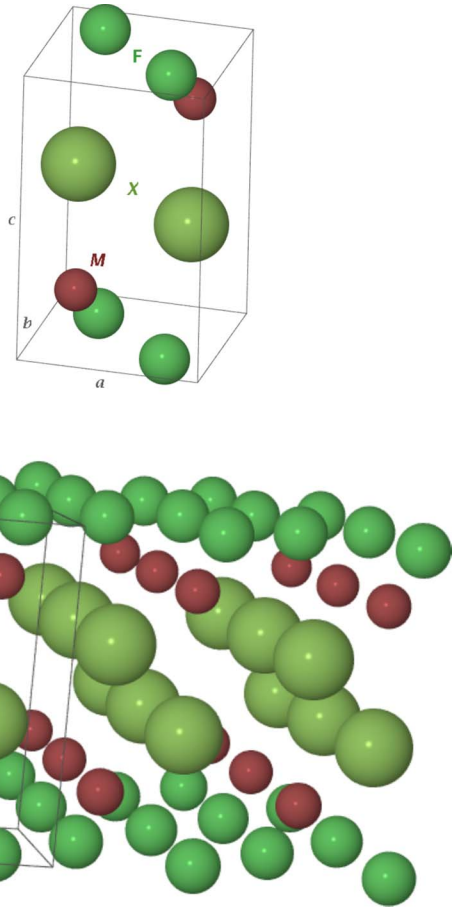

FIG. 1. (Color online) The tetragonal $P4/nmm$ Matlockite structure of the MFX alkaline-earth fluorohalides: the unit cell (top) and a $3\times3\times1$ supercell showing the layer stacking (bottom).

these compounds should be studied as well since their variations with pressure or chemical substitutions are good reporters of the induced structural changes. We have therefore undertaken a thorough investigation of the structural and vibrational properties of BaFCl under pressure and of the $Ba_{1-x}Sr_xFCl$ $(0\leq x\leq 1)$ system, based on density-functional theory (DFT) (Refs. 14 and 15) calculations performed within the local-density approximation (LDA) (Refs. 16 and 17) and the generalized gradient approximation (GGA).[18,19] As shown in this paper wherein we report our results, there is also an additional twofold interest in the study of these compounds. On the one hand, these compounds are experimentally well characterized and the comparison between our results and the available experimental data helps assess the performance of the theoretical approaches used. This is especially the case for the virtual-crystal approximation (VCA) (Refs. 20 and 21) used for the description of the $Ba_{1-x}Sr_xFCl$ system. On the other hand, the characterization of both BaFCl under pressure and the $Ba_{1-x}Sr_xFCl$ system allows to critically discuss the extent to which an equivalence can be established between physical and chemical pressures.

II. COMPUTATIONAL AND EXPERIMENTAL DETAILS

The $Ba_{1-x}Sr_xFCl$ compounds were studied using periodic DFT calculations performed with the ABINIT package,[22–24]

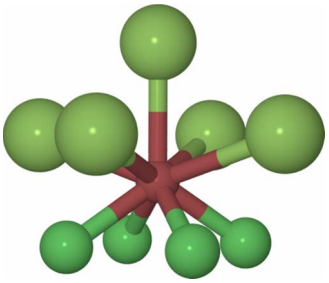

FIG. 2. (Color online) The ninefold coordination of M^{2+} in the tetragonal $P4/nmm$ Matlockite structure of the MFX alkaline-earth fluorohalides: a $[MF_4X_5]$ structural motif of C_{4v} site symmetry.

which is based on pseudopotentials and plane waves. We used optimized Rappe-Rabe-Kaxiras-Joannopoulos (RRKJ) pseudopotentials[25] in the separable Kleinman-Bylander form.[26] The pseudopotentials were generated thanks to the OPIUM program,[27] taking for the Ba atom scalar relativistic effects[28] into account. A $10\times10\times5$ k-point Monkhorst-Pack grid[29] was employed and the wave functions were expanded in plane waves up to a kinetic-energy cutoff of 40 hartree and 60 hartree for the GGA and LDA calculations, respectively. For the investigation of $Ba_{1-x}Sr_xFCl$ $(x>0)$, we used the VCA as implemented in ABINIT.[21] Phonons were calculated at the center of the Brillouin zone within density-functional perturbation theory.[30,31] In all calculations, the symmetry was kept fixed to the tetragonal space group $P4/nmm$: Ba^{2+} and Sr^{2+} are on a site $2c$ $(1/4,1/4,z_M)$, $(M=\mathrm{Ba,Sr})$; Cl^- is on a site $2c$ positions $(1/4,1/4,z_{Cl})$; and F^- on a site $2a$ (3/4, 1/4, 0). The phonon calculations confirmed that the calculated structures are stable. The symmetry analysis of the vibrational modes was performed with the ABINIT utility "getirrep.py," which makes use of the data available on the Bilbao Crystallographic Server.[32,33] Structure rendering was done with the JMOL (Refs. 34 and 35) and the V_SIM (Ref. 36) viewers.

Mixed $Ba_{1-x}Sr_xFCl$ compounds were prepared in batches of 0.5 g starting from $BaCl_2$, $SrCl_2$, BaF_2, and SrF_2 mixtures. The ground mixtures were heated for 2 h 30 min at 900 °C in a quartz tube under hydrogen flow, cooled to room temperature, reground and heated a second time for 2 h at 900 °C. The products phase composition and crystal size was analyzed using a Phillips X'Pert powder diffractometer (Cu $K\alpha$) and the software package TOPAS.[37] Raman spectra were obtained using a Kaiser Optical Holospec monochromator in conjunction with a liquid-nitrogen-cooled charge-coupled-device camera. The spectra were excited with 488 nm diode laser light (50 mW).

III. RESULTS AND DISCUSSION

A. Neat BaFCl compound

We will characterize first the zero-pressure structural and vibrational properties of BaFCl, then their pressure dependence.

1. BaFCl at zero pressure

The tetragonal $P4/nmm$ structure of BaFCl is determined by the lattice parameters a and c, and by the fractional coor-

TABLE I. LDA and GGA optimized structural parameters of BaFCl at zero pressure. The experimental values of these parameters at ambient pressure are given for comparison purpose.

	GGA	LDA	Expt.[a]
a (Å)	4.460	4.348	4.394
c (Å)	7.359	7.238	7.225
z_{Ba}	0.2029	0.2117	0.2049
z_{Cl}	0.6479	0.6463	0.6472

[a]Taken from Ref. 38.

dinates z_{Ba} and z_{Cl}. The LDA and GGA values found for these parameters at zero pressure are summarized in Table I along with their ambient-pressure experimental counterparts. Inspection of Table I shows that there is a pretty good agreement between the calculated and experimental structural parameters: the calculated structural parameters are indeed within 1–3 % of the experimental values.

With two formula units *per* unit cell, there are 18 ionic degrees of freedom. At the Γ point, according to group theory applied to the $P4/nmm$ group, the space which they span decomposes into 12 modes of the following symmetries:[39]

$$\Gamma_{18} = 2a_{1g} \oplus b_{1g} \oplus 3e_g \oplus 3a_{2u} \oplus 3e_u. \quad (1)$$

Six modes are Raman active ($2\times a_{1g}$, $1\times b_{1g}$, $3\times e_g$), four modes are IR active ($2\times a_{2u}$, $2\times e_u$), and the remaining a_{2u} and e_u modes are the acoustic modes. The calculated zero-pressure and the measured ambient-pressure frequencies of the vibrational modes are summarized in Table II. For both the Raman and IR modes, one notes a good agreement between the calculated and the measured frequencies.

TABLE II. Calculated zero-pressure frequencies of the vibration modes of BaFCl: LDA and GGA results (cm^{-1}). The experimental ambient-pressure frequencies are given for comparison purpose.

		LDA	GGA	Expt.
Raman-active modes				
$\nu(1e_g)$		77	83	89,[a,c] 82[b]
$\nu(1a_{1g})$		122	145	125,[a,c] 132[b]
$\nu(2e_g)$		130	147	142,[a,c] 143[b]
$\nu(2a_{1g})$		156	169	162,[a] 165,[b] 161[c]
$\nu(b_{1g})$		199	237	212,[a,c] 216[b]
$\nu(3e_g)$		237	277	247,[a,c] 251[b]
IR-active modes				
$\nu(1e_u)$	TO	107	129	130[c]
	LO	136	156	148[c]
$\nu(1a_{2u})$	TO	119	152	143[c]
	LO	182	200	197[c]
$\nu(2e_u)$	TO	188	231	210[c]
	LO	274	306	290[c]
$\nu(2a_{2u})$	TO	270	305	293[c]
	LO	319	360	340[c]

[a]Taken from Ref. 39.
[b]Taken from Ref. 40.
[c]Taken from Ref. 41.

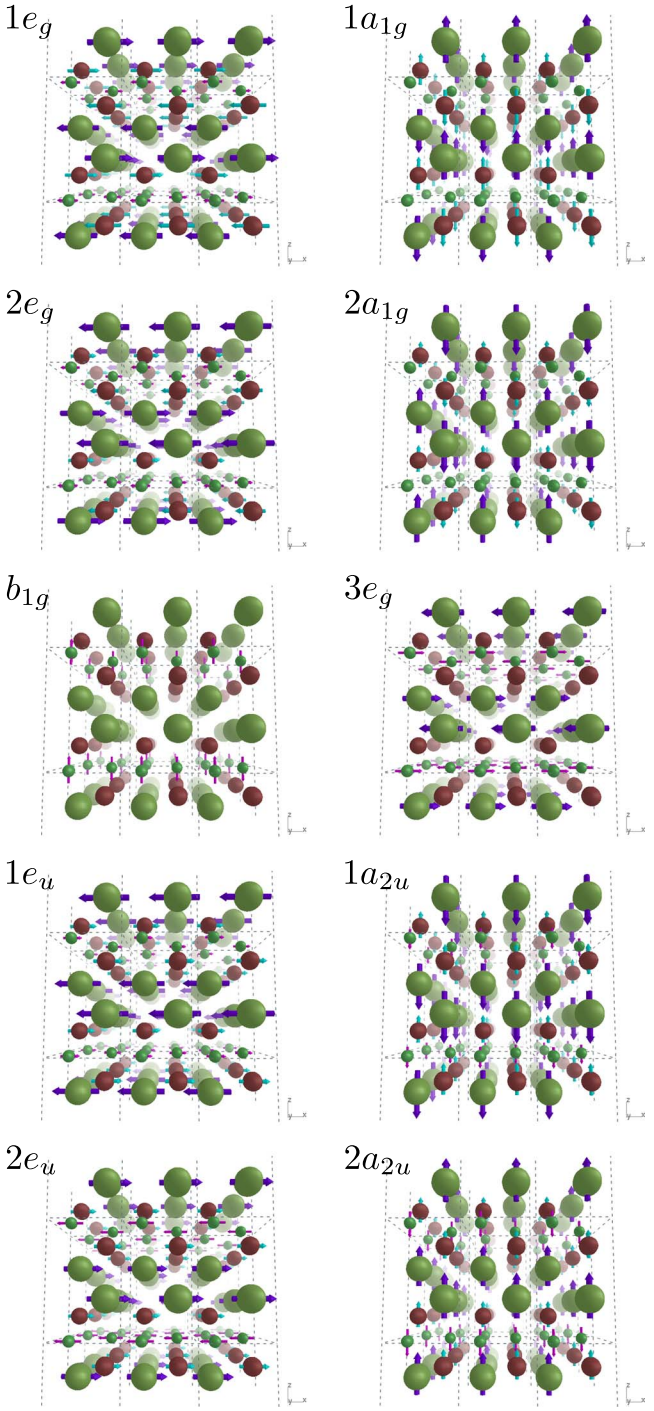

FIG. 3. (Color online) Eigendisplacements associated with the vibrational modes of BaFCl (GGA results at zero pressure).

The eigendisplacements associated with the vibrational modes of BaFCl are shown in Fig. 3. Actually, for the e_g and e_u modes, the eigendisplacements of their "x" components only are shown. The Raman-active modes can thus be depicted as follows. The lowest-frequency $1e_g$ is the shear mode characterized by the displacements in opposite directions of the adjacent Cl layers. The $2e_g$ mode can be associ-

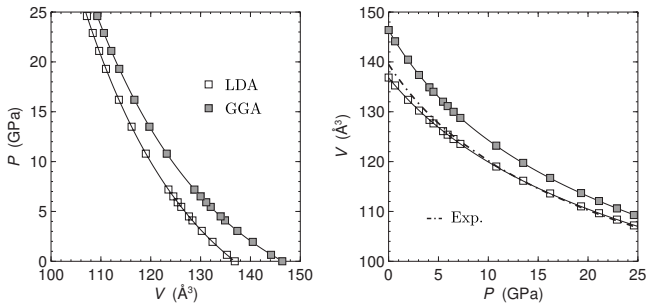

FIG. 4. *V-P* data (left) and *P-V* data (right) calculated for BaFCl and fitted using the Vinet and Murnaghan EoS, respectively: the calculated points are represented by squares and the fitting curves by solid lines. The dot-dashed line (right) represent the experimental Murnaghan EoS (Ref. 44).

ated with a Ba-Cl stretching motion. The $1a_{1g}$ and $2a_{1g}$ modes can be described as two breathing modes of the double Cl layers with the sandwiching Ba layers moving in the same or in the opposite direction, respectively. The b_{1g} and $3e_g$ modes correspond to the displacements of the F^- anions. As for the IR active modes, the lowest-frequency $1e_u$ mode corresponds to the shear mode characterized by an in-phase displacement of the Cl double layers. The $1a_{2u}$ mode corresponds to an in-phase movement of the Cl double layers in the direction opposite to the movement of the Ba layers. The $2e_u$ mode corresponds to the opposite displacements of the F atoms, on one side, and the Ba and Cl atoms, on the other side, parallel to the (x,y) plane. The $2a_{2u}$ mode can be described as an in-phase displacement of the Ba and Cl layers with the Cl layers moving in the opposite direction.

2. Influence of pressure

With increasing applied pressure, BaFCl undergoes two phase transitions. The first transition occurs at 10.8 GPa and brings the compound from the tetragonal to an orthorhombic phase of *Pnma* symmetry.[42] The second transition occurs at 21.1 GPa and leads to a monoclinic phase of $P2_1$ symmetry.[43] These transitions however are not complete and the different BaFCl phases actually coexist.[43] In this study, we have only considered the tetragonal $P4/nmm$ phase and investigated the influence of pressure on its structural and vibrational properties for applied pressures of up to 24.6 GPa. Thus, for a given target pressure P, we have, first, optimized the cell parameters and the internal positions, and then used this relaxed structure to calculate the Γ phonons frequencies.

The calculated volume-pressure (V-P) points are plotted in Fig. 4, which also shows the curves obtained from the fits of these data using the Vinet equation of state (EoS),[45]

$$P = 3B_0 \frac{(1-X)}{X^2} \exp[\eta(1-X)] \tag{2}$$

with

$$X = \left(\frac{V}{V_0}\right)^{1/3}, \tag{3}$$

$$\eta = \frac{3}{2}(B_0' - 1). \tag{4}$$

V_0 is the ambient-pressure equilibrium volume, B_0 is the bulk modulus at zero pressure

$$B_0 = -V_0 \left(\frac{\partial P}{\partial V}\right)_{T,P=P_0} \tag{5}$$

and B_0' is its pressure derivative

$$B_0' = \left(\frac{\partial B_0}{\partial P}\right)_{T,P=P_0}. \tag{6}$$

Figure 4 also shows the plots of the calculated P-V points and the curves obtained from their analysis with the Murnaghan EoS,[46]

$$V = V_0 \left(1 + \frac{B_0'}{B_0} P\right)^{-1/B_0'}. \tag{7}$$

Inspection of Fig. 4 shows that the pressure dependences of the cell volume can be satisfactorily analyzed using both the Vinet and Murnaghan EoS. The experimental Murnaghan EoS determined by Decremps *et al.*[44] is also plotted in Fig. 4. Given the uncertainties on the experimental data, and especially at high pressure (see Ref. 44), the agreement between the calculated and experimental Murnaghan EoS proves to be very good. One also notes in Fig. 4 that the difference between the GGA and LDA curves decreases with increasing pressure. This can be explained by the fact (i) that, due to the pressure-induced contraction of the cell, the electron gas becomes more homogeneous and (ii) that the GGA functional used recovers the behavior of the LDA functional when tending towards the slowly varying density limit, wherein the LDA is exact.

The calculated cell-parameter-pressure l-P data, $(l=a,c)$, have been analyzed using the modified Vinet EoS,

$$P = 3B_l \frac{(1-x)}{x^2} \exp[\eta(1-x)] \tag{8}$$

with

$$x = \left(\frac{l}{l_0}\right)^{1/3}, \tag{9}$$

$$\eta = \frac{3}{2}(B_l' - 1). \tag{10}$$

l_0 is the ambient-pressure equilibrium lattice parameter, B_l is the linear modulus,

$$B_l = -l_0 \left(\frac{\partial P}{\partial l}\right)_{T,P=P_0} \tag{11}$$

and B_l' is its pressure derivative $(l=a,c)$. As shown in Fig. 5, the pressure dependences of the cell parameters can be satisfactorily analyzed using a Vinet EoS. They could also be satisfactorily analyzed by using the modified Murnaghan EoS,

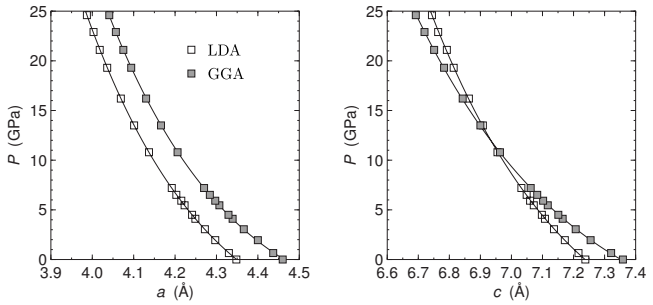

FIG. 5. l-P data calculated for BaFCl and fitted using the Vinet EoS ($l=a,c$): the calculated points are represented by squares and the fitting curves by solid lines.

$$l = l_0\left(1 + \frac{B_l'}{B_l}P\right)^{-1/B_l'} \tag{12}$$

to fit the calculated P-l points (data not shown).

The relative position in Fig. 5 of the LDA and GGA curves obtained for the a parameter reflects the fact that, compared to the GGA, the LDA tends to overbind. With increasing pressure, there is a decrease in the gap between these two curves. For the c parameter however, the LDA and GGA curves remain quite close and actually cross at $P \approx 11$ GPa.[47] This situation reflects the influence of the approximation used for dealing with the theoretical description of the anisotropic bonding in BaFCl.

In their recent study of mixed $PbFBr_{1-x}I_x$ crystals with the Matlockite structure, Hagemann *et al.*[48] have reported the characterization at the GGA level of the zero-pressure structure of the PbFI compound. The optimized value of the c parameter was found to be larger than the experimental value by as much as 11.4%, whereas the calculated and experimental values of the cell parameter a proved to agree to within 0.2%. They ascribed this discrepancy to the fact that the GGA functional, which we also use, tends to overestimate the separation between weakly interacting layers,[49] as attested for by the overestimation which they noticed for the I-I interlayer distance. However, such a large overestimation of the cell parameter c is not observed for our zero-pressure results (Table I), nor for the results of two recent zero-pressure DFT studies of BaFCl and SrFCl using LDA, GGA, and hybrid functionals.[50,51] That is, passing from the X=Cl halogen to the more polarizable X=I halogen allows to vary the bonding situation in the MFX family of compounds, and especially the weak bonding between the X layers along the c axis. This in turn helps question the accuracy of the DFT methods for the description of the bonding in the MFX compounds for varying bonding situations. More generally, because of the difficulties tied to the description of weak dispersive interactions within DFT, the treatment of layered structures using DFT methods is a challenging issue which is receiving much attention. For instance, in dealing with covalently bonded layers held together with dispersive interactions, Madsen *et al.* have shown that the inclusion of the kinetic-energy density in the M06-L meta-GGA gives such a type of functional enough flexibility to treat correctly both the covalent and the dispersive interactions in layered (see Ref. 52, and references therein). In this respect, we believe that the quality achieved for the description of the anisotropic bonding in the ionic layered MFX compounds at zero pressure and under applied pressure should be used as a severe criterion for assessing further modern functionals with regard to the treatment of layered structures.

Our results suggest that the LDA and GGA functionals tend to perform well for the description of BaFCl at zero and under applied pressure. This is also illustrated by the agreement which can be observed in Table III between the calculated values of the bulk and linear moduli and of their pressure derivatives, on one hand, and the most up-to-date experimental data of Decremps *et al.*,[44] on the other hand. Indeed, the values obtained at the LDA or at the GGA level using the Vinet and Murnaghan EoS are quite consistent with one another and compare satisfactorily with the experimental values. However, the agreement between experiment and theory proves to be better for the GGA results than for the LDA ones. This is especially the case for the linear modulus B_c which is strongly overestimated at the LDA level but is well reproduced at the GGA level. That is, the compressibility along the c axis ($\chi_c = 1/B_c$) is strongly underestimated at the LDA level. These last results suggest that the GGA functional performs better than the LDA functional for the overall description of BaFCl.

Figure 6 shows the calculated pressure dependencies of the Raman-active modes as well the experimental pressure dependencies determined by Sundarakannan *et al.*[43] for the

TABLE III. Bulk (B_0) and linear (B_a, B_c) moduli (in GPa) and their pressure derivatives (B_0', B_a', B_c') determined for BaFCl using the Vinet and Murnaghan EoS: LDA and GGA results. Experimental values are also given for comparison purposes.

	Vinet EoS		Murnaghan EoS		Expt.
	GGA	LDA	GGA	LDA	(Ref. 44)
B_0	40.0	53.7	42.1	55.5	45
B_0'	5.2	5.3	4.3	4.5	5.2
B_a	115.6	148.9	123.1	154.2	132
B_a'	15.5	15.0	12.9	13.0	18
B_c	133.6	198.5	133.9	200.7	139
B_c'	14.5	16.1	13.0	14.5	10

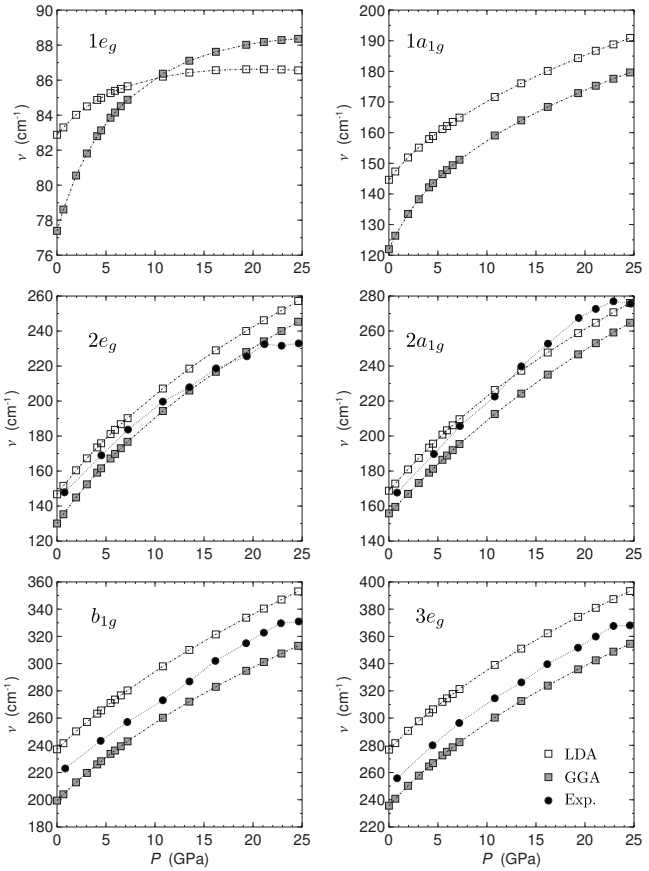

FIG. 6. Pressure dependencies of the frequencies of the Raman-active modes of BaFCl: LDA and GGA results. Available experimental data are shown for comparison purposes (Ref. 43). Lines only serve as guides for eyes.

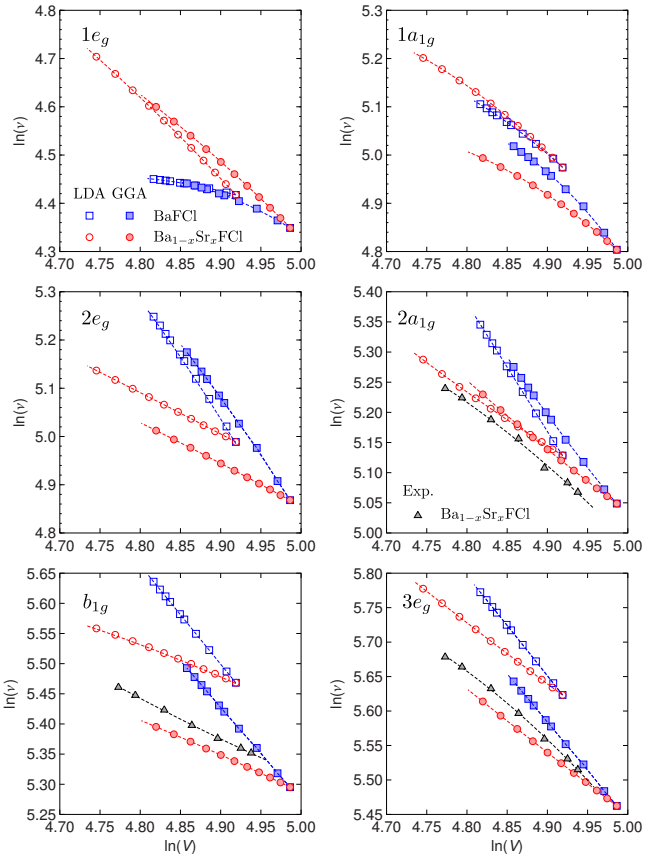

FIG. 7. (Color online) Predicted LDA and GGA volume dependencies of the frequencies of the Raman-active modes in BaFCl under pressure and under Ba→Sr substitution at zero pressure: plots of $\ln(\nu)$ versus $\ln(V)$. The experimental data determined in this study for the mixed $Ba_{1-x}Sr_xFCl$ crystals at ambient pressure are also shown. The dashed lines represent the quadratic fits of the calculated and experimental data.

$2e_g$, $2a_g$, b_{1g}, and $3e_g$ modes. A good agreement is observed between the calculated and the experimentally available data. The LDA and GGA results are consistent with one another, and except for the $1e_g$ mode, the calculated GGA frequencies remain lower than the calculated LDA frequencies for the considered pressure range, and exhibit comparable pressure dependencies. For the $1e_g$ mode, this ordering gets reversed with increasing pressure at ≈11 GPa. Such an ordering reversal was also found for the LDA and GGA pressure dependencies of the c parameter. This suggests that the pressure dependency of the $1e_g$ frequency is quite strongly sensitive to the bonding-type anisotropy in BaFCl and especially the bonding between the double Cl layers. This is consistent with the fact that the $1e_g$ mode is the shear mode characterized by the displacement of adjacent Cl layers in opposite directions (Fig. 3). It would therefore be interesting to have the experimentally determined pressure dependence of the $1e_g$ frequency for comparison.

The pressure dependencies of the frequencies of the IR-active modes are not known experimentally. We have determined them at the LDA and GGA levels. In the considered pressure range, the GGA frequencies remain lower than the LDA ones. Furthermore, the LDA and GGA pressure dependencies of the IR frequencies are actually quite similar. From this, it especially follows that the LO-TO splitting is predicted at both theoretical levels to exhibit a weak dependency on the applied pressure (see supplementary material[53]).

The mode Grüneisen parameter γ_i represents the volume dependence of the frequency ν_i of the ith vibrational mode,

$$\gamma_i = -\left.\frac{\partial \ln \nu_i}{\partial \ln V}\right|_{T,P_0} \tag{13}$$

and it is related to the pressure dependence of the frequency through the bulk modulus B_0 according to

$$\gamma_i = B_0\left(\frac{\partial \ln \nu_i}{\partial P}\right). \tag{14}$$

Figure 7 shows the plot of $\ln(\nu)$ versus $\ln(V)$ for the Raman-active modes.

From the quadratic fits of the $[\ln(V), \ln(\nu)]$ data shown in Fig. 7 and Eq. (13), the mode Grüneisen parameters of the Raman-active modes have been determined. We have proceeded similarly for determination of the Grüneisen parameters of the IR-active modes (data not shown). The results are summarized in Table IV, with the experimental values of

TABLE IV. Mode Grüneisen parameters calculated at the LDA and GGA levels for BaFCl from the determination of the pressure dependencies of its cell volume and vibrational frequencies. Available experimental data are also given.

		LDA	GGA	Expt.
Raman-active modes				
γ_{1e_g}		0.45	1.02	
$\gamma_{1a_{1g}}$		1.52	2.26	
γ_{2e_g}		2.74	2.62	2.00[a]
$\gamma_{2a_{1g}}$		2.14	1.60	1.84[a]
$\gamma_{b_{1g}}$		1.64	1.53	1.16[a]
γ_{3e_g}		1.50	1.43	1.17[a]
IR-active modes				
γ_{1e_u}	TO	3.20	3.31	
	LO	2.24	2.19	
$\gamma_{1a_{2u}}$	TO	2.91	3.59	
	LO	1.70	1.67	
γ_{2e_u}	TO	1.67	1.94	
	LO	1.12	1.11	
$\gamma_{2a_{2u}}$	TO	1.30	1.11	
	LO	1.19	1.01	

[a]Taken from Ref. 43: the experimental mode Grüneisen parameters were determined from the measured pressure dependencies of the frequencies using Eq. (14) and $\chi_0=1/B_0=0.0225$ GPa^{-1}.

the mode Grüneisen parameters of the $2e_g$, $2a_{1g}$, b_{1g}, and $3e_g$ Raman-active modes as determined by Sundarakkannan *et al.*[43] The comparison of these experimental values with the calculated ones shows that there is for these modes a good agreement between experiment and theory, the agreement being actually better at the GGA level than at the LDA level. From this, we infer that the GGA values of the $1e_g$ and $1a_{1g}$ Grüneisen parameters are probably more reliable than the LDA ones. Note that, contrarily to what is observed for the Grüneisen parameters of the other Raman-active modes, the GGA values found for $1e_g$ and $1a_{1g}$ Grüneisen parameters are larger than the LDA counterparts. Still, the Grüneisen parameter of the $1e_g$ shear mode is predicted at both levels to be the smallest one, when considering the Raman-active modes and also the IR-active modes. This is consistent with the fact that the frequency of this mode is predicted to exhibit the weakest pressure dependence (see Fig. 6 and supplementary material[53]).

In passing to the IR-active modes, one notes that the consistency between the LDA and GGA values of the Grüneisen parameters improves, and that the Grüneisen parameters of the TO phonons are predicted at both theoretical levels to be larger than those of the LO phonons. The sensitivity of the description of the weak interactions between the Cl layers to the theoretical level probably explains the difference in the consistency between the LDA and GGA γ_i values on passing from the Raman to the IR modes. Indeed, the Raman modes involve the displacements of the adjacent Cl layers in opposite directions whereas the IR modes involve in-phase displacements of these layers (Fig. 3). Finally, one notes in Table IV that the mode Grüneisen parameters are all of the same order of magnitude with the exception of the LDA value of γ_{1e_g} which is most likely underestimated. This reflects the relatively small anisotropy of the compressibility of BaFCl, as determined experimentally[44] and confirmed here at the GGA level (Table III). This also reflects the fact that there is no given void in the structure of BaFCl which is being filled considerably faster than others, as opposed to what we have recently found for Ca_2RuH_6, for instance.[54]

B. $Ba_{1-x}Sr_xFCl$ system

The $Ba_{1-x}Sr_xFCl$ system forms for all Sr/Ba ratios complete solid solutions which crystallize in the tetragonal $P4/nmm$ space group.[9] For its study within the VCA used, the pseudopotential of a virtual alkaline-earth atom was constructed as the weighted sum of the pseudopotentials of the Ba and Sr atoms,[21]

$$\hat{V}^{psp}_{\mathrm{VCA}}[x] = (1-x)\hat{V}^{psp}_{\mathrm{Ba}} + x\hat{V}^{psp}_{\mathrm{Sr}} \tag{15}$$

and the mass m_{VA} of the virtual atom, which is needed for the determination of the phonons, was taken as the average mass,

$$m_{\mathrm{VA}}[x] = (1-x)m_{\mathrm{Ba}} + xm_{\mathrm{Sr}}. \tag{16}$$

The variation in the lattice parameters with the chemical composition has been recorded for $0 \leq x \leq 1$. Our results compare very well with previously reported experimental data (see Ref. 9, and references therein). For instance, for $x=0.2$, we have $a=4.351$ Å and $c=7.175$ Å, and parameter values of $a=4.338$ Å and $c=7.158$ Å have been determined for the mixed crystal with $x=0.19$.[9] Our calculated and experimental composition dependencies of the cell parameters and volume are plotted in Fig. 8. On notes a fairly good agreement between experiment and theory: the LDA and GGA curves indeed parallel quite nicely the experimental curves and the differences reflect the usual LDA underestimate and GGA overestimate of the structural parameters. As shown in Fig. 9, the good agreement observed between experiment and theory extends also to the composition dependencies of the frequencies of the Raman-active modes $2a_{1g}$, b_{1g}, and $3e_g$. This makes us quite confident about the quality of the composition dependencies predicted for the frequencies of the other Raman modes (Fig. 9) and for the frequencies of the IR modes (see supplementary material[53]).

Upon the substitution of the Ba^{2+} ions by the Sr^{2+} ions of smaller radius, the lattice shrinks and the vibrational frequencies increase, as observed for BaFCl under applied pressure. The decrease in the cell volume observed on passing from BaFCl to SrFCl actually corresponds to the one achieved for BaFCl by applying an external pressure of about 10 GPa. However, as this can be inferred from the comparison of Figs. 4, 5, and 8, a formal equivalence cannot be established here between the chemical and the physical pressure. Indeed, the $V=V(P)$ and $V=V(x)$ curves have opposite curvatures, likewise for the $l=l(P)$ and $l=l(x)$ curves ($l=a,b$). The differences between the effects of the physical and the chemical pressure are also emphasized by the plots in Fig. 7 of the volume dependencies of the Raman frequencies: $\ln(\nu) = f[\ln(V)]$ for BaFCl under pressure and for the $Ba_{1-x}Sr_xFCl$

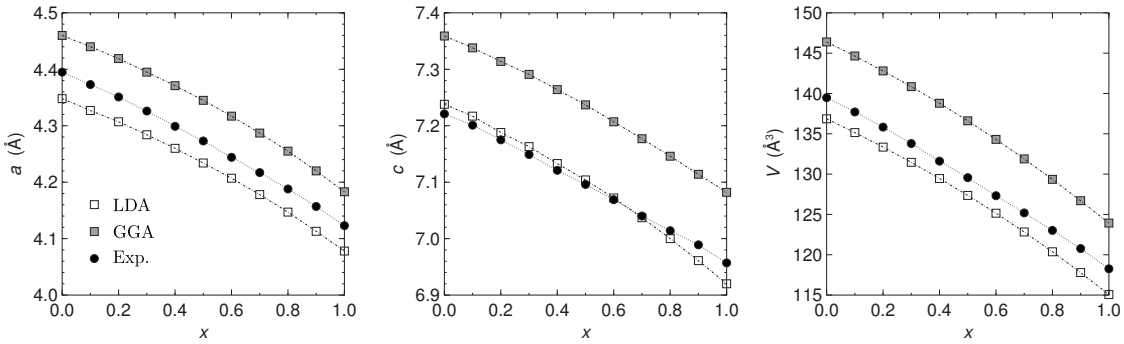

FIG. 8. The $Ba_{1-x}Sr_xFCl$ system at zero pressure: calculated LDA and GGA dependencies on the chemical composition x of the cell parameters a and b and of the cell volume V. Experimental ambient-pressure data are also plotted for comparison purposes (Ref. 9). The lines only serve as guides for eyes.

system. The mode Grüneisen parameters provide a dimensionless measure of the response of a system to compression. Its definition given by Eq. (17) can be extended as follows:

$$\tilde{\gamma}_i = -\left.\frac{\partial \ln \nu_i}{\partial \ln V}\right|_{T,P_0,x=0} \tag{17}$$

in order to quantify the response to the compression induced by the substitution of the Ba^{2+} ions by the Sr^{2+} ions. Table V summarizes the values of $\tilde{\gamma}_i$ obtained from the DFT calculations and our measurements. The LDA and GGA $\tilde{\gamma}_i$ values are quite consistent with one another, especially for the IR-active modes, and a good agreement is also observed between experiment and theory for the Raman-active modes $2a_{1g}$, b_{1g}, and $3e_g$.

The $\tilde{\gamma}_i$ values of the IR-active modes fall all within the 0.5–0.7 narrow range and, for a given IR mode, they are quite similar for the TO and LO phonons. Furthermore, they are similar to $\tilde{\gamma}_{b_{1g}}$. This suggests that the compression induced by the chemical substitution affects similarly the IR modes and the Raman b_{1g} mode, which all are characterized by in-phase displacements of the atomic planes of same natures. The $\tilde{\gamma}_i$ values are larger for the other Raman modes characterized by displacements of these atomic planes in opposite directions, the largest $\tilde{\gamma}_i$ value being predicted for the $1e_g$ shear mode. As observed for the γ_i mode Grüneisen parameters (Table IV), the $\tilde{\gamma}_i$ values are of the same order of magnitude. Hence, as for BaFCl under pressure, the compression induced by the chemical substitution occurs with a small anisotropy. But, beside this similitude, the comparison of Tables IV and V shows that the responses of BaFCl to the physically induced and the chemically induced compression do differ. That is, the external pressure and the chemical substitution affect differently the local structures of the crystal or, to be more precise here, the variations in the vibrating volumes associated to the vibrational modes.[55]

Finally, we have also studied the stability of the $Ba_{1-x}Sr_xFCl$ system by calculating the energy of formation $\Delta E_f(x)$ associated to the reaction of mixing

$$(1-x)\mathrm{BaFCl} + x\mathrm{SrFCl} \rightarrow \mathrm{Ba}_{1-x}\mathrm{Sr}_x\mathrm{FCl}. \tag{18}$$

ΔE_f, which gives an estimate of the enthalpy of mixing at $T=0$ when neglecting the zero-point corrections, is plotted against the chemical composition parameter x in Fig. 10 for $x \in [0,1]$. The LDA and GGA curves have both a bell shape and are nearly superimposed. Their inspection shows that the mixing is not energetically favored ($\Delta E_f > 0$ for $x \neq 0$ and $x \neq 1$), and that ΔE_f increases with x, reaches a maximum at $x_{\min} \approx 0.6$, and then decreases to zero. Differential thermal analysis measurements on $Ba_{1-x}Sr_xFCl$ and related systems[56] showed that these systems are fully miscible and exhibit a minimum melting point (see Fig. 10). Furthermore, crystal

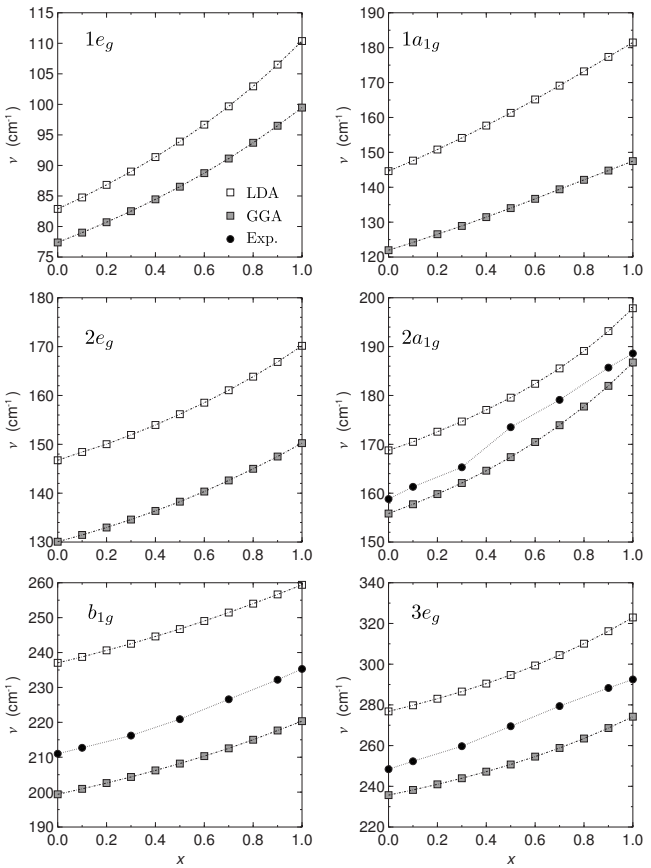

FIG. 9. The $Ba_{1-x}Sr_xFCl$ system at zero pressure: calculated LDA and GGA dependencies on the chemical composition x of the frequencies of the Raman-active modes. The data recorded at ambient pressure for the $2a_{1g}$, b_{1g}, and $3e_g$ modes are also plotted. The lines only serve as guides for eyes.

TABLE V. Mode Grüneisen parameters calculated at the LDA and GGA levels for the $Ba_{1-x}Sr_xFCl$ system from the determination of the chemical composition dependencies of its cell volume and vibrational frequencies. The mode Grüneisen parameters determined from our experiments are also given.

		LDA	GGA	Expt.
Raman-active modes				
$\tilde{\gamma}_{1e_g}$		1.80	1.67	
$\tilde{\gamma}_{1a_{1g}}$		1.67	1.52	
$\tilde{\gamma}_{2e_g}$		0.95	0.90	
$\tilde{\gamma}_{2a_{1g}}$		0.82	0.99	1.24
$\tilde{\gamma}_{b_{1g}}$		0.59	0.64	0.61
$\tilde{\gamma}_{3e_g}$		0.86	0.88	1.21
IR-active modes				
$\tilde{\gamma}_{1e_u}$	TO	0.48	0.54	
	LO	0.48	0.54	
$\tilde{\gamma}_{1a_{2u}}$	TO	0.66	0.61	
	LO	0.62	0.60	
$\tilde{\gamma}_{2e_u}$	TO	0.54	0.59	
	LO	0.60	0.64	
$\tilde{\gamma}_{2a_{2u}}$	TO	0.54	0.56	
	LO	0.62	0.65	

structure determinations[9,56] and Raman spectra showed that in these solids, the disorder appears to be fully statistical. Indeed, the atomic displacement parameters for the sites occupied statistically by the Ba and Sr atoms remain similar to those of pure SrFCl and BaFCl, and the Raman spectra show no breakdown of selection rules or additional bands, as were observed for $BaFBr_{1-y}I_y$ (Ref. 57) and $PbFBr_{1-y}I_y$.[48] A fully miscible system with a minimum melting point can be described by using for the solid and liquid phases regular solution models (i.e., with an ideal entropy contribution and a nonideal (nonzero) enthalpy contribution to their Gibbs free energy of mixing). The departure from ideality of the liquid phase is in this case more negative than that of the solid phase.[58] Accordingly, the melting point T_m correlates negatively with the enthalpy of formation of the mixed solid. This negative correlation appears indeed in Fig. 10. We may therefore draw the conclusion that the mixing entropy of the fully miscible $Ba_{1-x}Sr_xFCl$ system is similar in the solid and liquid phases, and that mixing destabilizes the solid phase by a larger amount than the liquid phase.

In summary, DFT calculations performed at the LDA and GGA levels within the VCA have allowed us to gain insight into the structural, vibrational, and thermochemical properties of the $Ba_{1-x}Sr_xFCl$ solid solution.

IV. CONCLUDING REMARKS

We have characterized the structural and vibrational properties of BaFCl under pressure as well as those of the $Ba_{1-x}Sr_xFCl$ ($0 \le x \le 1$) system by carrying out periodic DFT calculations at the LDA and GGA levels. These results show that the application of an external pressure and the substitution of the Ba^{2+} ions by the Sr^{2+} ions similarly lead to a contraction of the lattice parameters and an increase in the vibrational frequencies. However, the comparison of the calculated mode Grüneisen parameters shows that, for the investigated systems, the effects of physical and chemical pressures do actually differ.

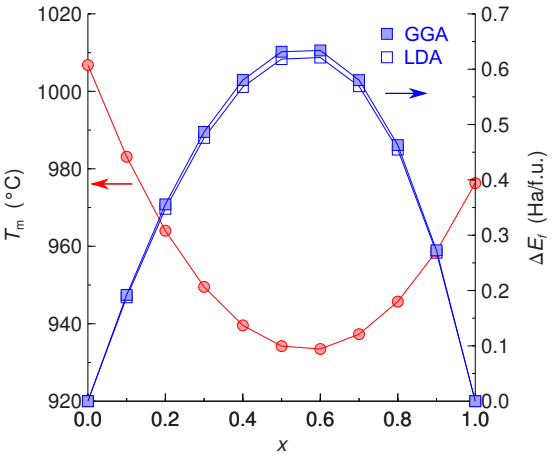

FIG. 10. (Color online) The $Ba_{1-x}Sr_xFCl$ system: dependence on the composition x in Sr of the temperature of melting at ambient pressure (Ref. 56) (in °C) and of the energy of formation (in hartree per formula unit) associated to the reaction of mixing at zero pressure: $(1-x)BaFCl+xSrFCl \rightarrow Ba_{1-x}Sr_xFCl$.

The results of the LDA and GGA calculations show overall a good agreement with experiment, as assessed by their comparison with previously reported experimental data for

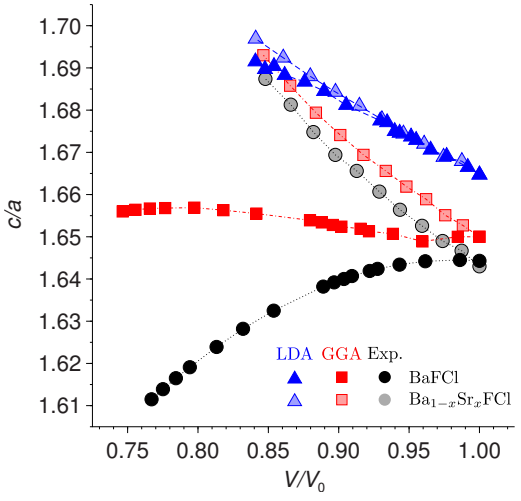

FIG. 11. (Color online) Calculated and experimental variations in BaFCl and $Ba_{1-x}Sr_xFCl$ of the ratio c/a of the cell parameters with the relative cell volume V/V_0, where V_0 is the calculated zero-pressure or the experimental ambient-pressure equilibrium volume of BaFCl. The reported structural changes result from the application of an external pressure in the case of BaFCl, and, for $Ba_{1-x}Sr_xFCl$, from the variation in the chemical composition of the solid solution at zero or, experimentally, at ambient pressure. The experimental curve plotted for BaFCl was derived from the experimental Murnaghan EoS determined by Decremps *et al.* (Ref. 44) for a and c (see Table III for the values used for the linear moduli and their pressure derivatives).

BaFCl and new experimental data for $Ba_{1-x}Sr_xFCl$. The LDA and GGA methods are thus shown to perform equally well for the description within the VCA of the structural and vibrational properties of the $Ba_{1-x}Sr_xFCl$ system but also of its stability. However they prove to perform differently for the description of BaFCl under pressure, the GGA method outperforming the LDA method. In order to further assess the performances of the two methods for the description of physical pressure effects in BaFCl and chemical pressure effects in $Ba_{1-x}Sr_xFCl$, we compare in Fig. 11 the calculated and experimental variations in the ratio c/a of the cell parameters with the relative cell volume V/V_0, where V_0 is the calculated zero-pressure or the experimental ambient-pressure equilibrium volume of BaFCl.

The inspection of the experimental curves shows that, for both BaFCl and the $Ba_{1-x}Sr_xFCl$ system, the ratio c/a exhibits small but noticeable variations with V/V_0, which attest for the small anisotropy of the physically or chemically induced compression. Furthermore these experimental curves have opposite curvatures. This demonstrates once more the nonequivalence of the physical and chemical pressure effects in the investigated compounds. This last conclusion cannot be drawn from the LDA curves which, taken alone, would actually have led to the opposite conclusion. In contrast, the GGA curves reproduce quite well the experimental trends. Given the large uncertainties on the experimental values of the c/a and V/V_0 ratios at high pressures (see Ref. 44), there is in fact a very good agreement between the GGA and experimental curves. Our results thus give the GGA method as the preferred method for the description of the BaFCl and $Ba_{1-x}Sr_xFCl$ compounds. More generally, with the large variety of bonding-type anisotropies which they exhibit, the numerous experimental data available for the alkaline-earth fluorohalides make them ideal benchmark systems for assessing the performances of the DFT methods for the description of layered compounds.

ACKNOWLEDGMENTS

This work has benefited from the financial support of the Swiss National Science Foundation. We thank the Swiss National Supercomputing Centre (CSCS) for the calculation resources allocated under project ID 103. The authors thank A. Rief (TU Wien) for help with sample preparation and x-ray characterization of the mixed crystals.

*Corresponding author; max.lawson@unige.ch

[1] A. R. Lakshmanan, Phys. Status Solidi A **153**, 3 (1996).
[2] K. Takahashi, J. Lumin. **100**, 307 (2002).
[3] H. von Seggern, Braz. J. Phys. **29**, 254 (1999).
[4] H. Riesen and W. A. Kaczmarek, Inorg. Chem. **46**, 7235 (2007).
[5] R. Jaaniso and H. Bill, Europhys. Lett. **16**, 569 (1991).
[6] R. Jaaniso, H. Hagemann, F. Kubel, and H. Bill, Chimia **46**, 133 (1992).
[7] Y. R. Shen, T. Gregorian, and W. B. Holzapfel, High Press. Res. **7**, 73 (1991).
[8] P. Comodi and P. F. Zanazzi, J. Appl. Crystallogr. **26**, 843 (1993).
[9] H. Hagemann, F. Kubel, and H. Bill, Mater. Res. Bull. **28**, 353 (1993).
[10] A. Hauser, N. Amstutz, S. Delahaye, A. Sadki, S. Schenker, R. Sieber, and M. Zerara, Struct. Bonding (Berlin) **106**, 81 (2004).
[11] A. Vargas, A. Hauser, and L. M. Lawson Daku, J. Chem. Theory Comput. **5**, 97 (2009).
[12] M. Sugi, Y. Matsumoto, N. Kimura, T. Komatsubara, H. Aoki, T. Terashima, and S. Uji, Phys. Rev. Lett. **101**, 056401 (2008).
[13] S. A. J. Kimber, A. Kreyssig, Y.-Z. Zhang, H. O. Jeschke, R. Valentí, F. Yokaichiya, E. Colombier, J. Yan, T. C. Hansen, T. Chatterji, R. J. McQueeney, P. C. Canfield, A. I. Goldman, and D. N. Argyriou, Nature Mater. **8**, 471 (2009).
[14] P. Hohenberg and W. Kohn, Phys. Rev. **136**, B864 (1964).
[15] W. Kohn and L. J. Sham, Phys. Rev. **140**, A1133 (1965).
[16] J. C. Slater, *Quantum Theory of Molecules and Solids*, International Series in Pure and Applied Physics Vol. 4 (McGraw-Hill, New York, 1974).
[17] J. P. Perdew and Y. Wang, Phys. Rev. B **45**, 13244 (1992).
[18] J. P. Perdew, K. Burke, and M. Ernzerhof, Phys. Rev. Lett. **77**, 3865 (1996).
[19] J. P. Perdew, K. Burke, and M. Ernzerhof, Phys. Rev. Lett. **78**, 1396 (1997).
[20] L. Nordheim, Ann. Phys. **401**, 607 (1931).
[21] P. Ghosez, D. Desquesnes, X. Gonze, and K. M. Rabe, *Fundamental Physics of Ferroelectrics 2000*, AIP Conf. Proc. No. 535 (AIP, New York, 2000), p. 102.
[22] X. Gonze, J.-M. Beuken, R. Caracas, F. Detraux, M. Fuchs, G.-M. Rignanese, L. Sindic, M. Verstraete, G. Zerah, F. Jollet, M. Torrent, A. Roy, M. Mikami, P. Ghosez, J.-Y. Raty, and D. Allan, Comput. Mater. Sci. **25**, 478 (2002).
[23] X. Gonze, G.-M. Rignanese, M. Verstraete, J.-M. Beuken, Y. Pouillon, R. Caracas, F. Jollet, M. Torrent, G. Zerah, M. Mikami, P. Ghosez, M. Veithen, J.-Y. Raty, V. Olevano, F. Bruneval, L. Reining, R. Godby, G. Onida, D. R. Hamann, and D. C. Allan, Z. Kristallogr. **220**, 558 (2005).
[24] ABINIT code, a common project of the Université Catholique de Louvain, Corning Incorporated, the Université de Liège, the Commissariat á l'Energie Atomique, Mitsubishi Chemical Corp., the Ecole Polytechnique Palaiseau, and other contributors, http://www.abinit.org
[25] A. M. Rappe, K. M. Rabe, E. Kaxiras, and J. D. Joannopoulos, Phys. Rev. B **41**, 1227 (1990).
[26] L. Kleinman and D. M. Bylander, Phys. Rev. Lett. **48**, 1425 (1982).
[27] http://opium.sourceforge.net (last visited: 2010-05-04).
[28] I. Grinberg, N. J. Ramer, and A. M. Rappe, Phys. Rev. B **62**, 2311 (2000).
[29] H. J. Monkhorst and J. D. Pack, Phys. Rev. B **13**, 5188 (1976).
[30] X. Gonze and C. Lee, Phys. Rev. B **55**, 10355 (1997).
[31] X. Gonze, Phys. Rev. B **55**, 10337 (1997).
[32] M. I. Aroyo, J. M. Perez-Mato, C. Capillas, E. Kroumova, S. Ivantchev, G. Madariaga, A. Kirov, and H. Wondratschek, Z.

Kristallogr. **221**, 15 (2006).
[33] M. I. Aroyo, A. Kirov, C. Capillas, J. M. Perez-Mato, and H. Wondratschek, Acta Crystallogr., Sect. A: Found. Crystallogr. **62**, 115 (2006).
[34] JMOL: an open-source Java viewer for chemical structures in three dimensions, http://www.jmol.org (accessed Feb. 14, 2010).
[35] B. McMahon and R. M. Hanson, J. Appl. Crystallogr. **41**, 811 (2008).
[36] D. Caliste, L. Billard, and O. D'Hastier, http://www-drfmc.cea.fr/sp2m/L_Sim/V_Sim/ (accessed May 4, 2010).
[37] A. Coelho, TOPAS-ACADEMIC, http://www.topas-academic.net/, accessed May 4 2010.
[38] M. Sauvage, Acta Crystallogr., Sect. B: Struct. Crystallogr. Cryst. Chem. **30**, 2786 (1974).
[39] J. F. Scott, J. Chem. Phys. **49**, 2766 (1968).
[40] D. Nicollin and H. Bill, J. Phys. C **11**, 4803 (1978).
[41] M. Sieskind, M. Ayadi, and G. Zachmann, Phys. Status Solidi B **136**, 489 (1986).
[42] N. Subramanian, N. V. C. Shekara, P. C. Sahua, K. G. Rajana, and A. L. Ruoff, Physica B **351**, 5 (2004).
[43] B. Sundarakannan, T. R. Ravindran, R. Kesavamoorthy, and S. V. M. Satyanarayana, Solid State Commun. **124**, 385 (2002).
[44] F. Decremps, M. Fischer, A. Polian, J. P. Itié, and M. Sieskind, Phys. Rev. B **59**, 4011 (1999).
[45] P. Vinet, J. H. Rose, J. Ferrante, and J. R. Smith, J. Phys.: Condens. Matter **1**, 1941 (1989).
[46] F. D. Murnaghan, Proc. Natl. Acad. Sci. U.S.A. **30**, 244 (1944).
[47] Remarkably, this pressure coincides with the pressure at which the first phase transition is observed for BaFCl. This raises the question as to know whether this crossing and its occurrence near the transition pressure is accidental or rooted in the very nature of the LDA and GGA. We will not address this question here as it actually deserves an other whole study.
[48] H. Hagemann, A. Rief, F. Kubel, J. L. M. van Mechelen, F. Tran, and P. Blaha, J. Phys.: Condens. Matter **19**, 036214 (2007).
[49] H. Rydberg, M. Dion, N. Jacobson, E. Schröder, P. Hyldgaard, S. I. Simak, D. C. Langreth, and B. I. Lundqvist, Phys. Rev. Lett. **91**, 126402 (2003).
[50] M. Mérawa, Y. Noël, B. Civalleri, R. Brown, and R. Dovesi, J. Phys.: Condens. Matter **17**, 535 (2005).
[51] P. Labéguerie, F. Pascale, M. Mérawa, C. Zicovich-Wilson, N. Makhouki, and R. Dovesi, Eur. Phys. J. B **43**, 453 (2005).
[52] G. K. H. Madsen, L. Ferrighi, and B. Hammer, J. Phys. Chem. Lett. **1**, 515 (2010).
[53] See supplementary material at http://link.aps.org/supplemental/10.1103/PhysRevB.82.024108 for the following supporting information: (A) plots of the pressure dependences of the IR frequencies of BaFCl and of the composition dependences of the IR frequencies of $Ba_{1-x}Sr_xFCl$ at $P=0$ (Figs. S1 and S2); (B) fourth-order polynomial parametrization of the pressure dependences of the vibrational frequencies of BaFCl and of the chemical composition dependences of the vibrational frequencies of $Ba_{1-x}Sr_xFCl$ (Tables S1–S4); and (C) quadratic fits of the volume dependences of the vibrational frequencies $\{\ln(\nu) = f[\ln(V)]\}$ of BaFCl under pressure and of $Ba_{1-x}Sr_xFCl$ at zero or ambient pressure (Tables S5–S7).
[54] We have recently reported the study of the pressure dependence of the structural and vibrational properties of the ternary metal hydride Ca_2RuH_6, which crystallizes in the cubic $Fm\bar{3}m$ space group and is made of octahedral $[RuH_6]^{4-}$ molecular units stabilized the Madelung field of by the Ca^{2+} cations (Ref. 59). The Ru atoms sit on the faces and the apexes of the conventional cell, the Ru-H bond are parallel to the axes of the conventional cell, and the Ca^{2+} cations occupy the tetrahedral sites. Under applied pressure, the Ru-H bond length was found to decrease slower than the cell parameter. That is, the void between the octahedra is being filled faster than the octahedra are getting contracted. As a consequence, the Grüneisen parameters of the Ru-H stretching modes are one order of magnitude smaller than those of the bending and librational modes of the $[RuH_6]^{4-}$ octahedra and those of the lattice translational modes. Furthermore, the largest Grüneisen parameter was found for the librational mode of the octahedra, thus reflecting the strong sensitivity of this mode to the available void.
[55] A. M. Hofmeister and H. k. Mao, Proc. Natl. Acad. Sci. U.S.A. **99**, 559 (2002).
[56] H. Hagemann, P. Tissot, D. Lovy, F. Kubel, and H. Bill, J. Therm Anal. Calorim. **57**, 193 (1999).
[57] J. M. Rey, H. Bill, H. Hagemann, and F. Kubel, Phys. Rev. B **72**, 184107 (2005).
[58] R. T. DeHoff, *Thermodynamics in Materials Science* (McGraw-Hill, New York, 1993).
[59] L. M. Lawson Daku and H. Hagemann, Phys. Rev. B **76**, 014118 (2007).